Diffuse reflectance spectroscopy sensor to differentiate between glial tumor and healthy brain tissue

A proof-of-concept study

Skyrman, Simon; Burström, Gustav; Lai, Marco; Manni, Francesca; Hendriks, Benno; Frostell, Arvid; Edström, Erik; Persson, Oscar; Elmi-Terander, Adrian

DOI
10.1364/BOE.474344

Publication date
2022

Document Version
Final published version

Published in
Biomedical Optics Express

Citation (APA)
Skyrman, S., Burström, G., Lai, M., Manni, F., Hendriks, B., Frostell, A., Edström, E., Persson, O., & Elmi-Terander, A. (2022). Diffuse reflectance spectroscopy sensor to differentiate between glial tumor and healthy brain tissue: A proof-of-concept study. *Biomedical Optics Express*, *13*(12), 6470-6483. https://doi.org/10.1364/BOE.474344

Research Article | Vol. 13, No. 12 / 1 Dec 2022 / Biomedical Optics Express 6470
Biomedical Optics EXPRESS

Diffuse reflectance spectroscopy sensor to differentiate between glial tumor and healthy brain tissue: a proof-of-concept study

SIMON SKYRMAN,[1,2,*] GUSTAV BURSTRÖM,[1,2] MARCO LAI,[3,4] FRANCESCA MANNI,[4] BENNO HENDRIKS,[3,5] ARVID FROSTELL,[1,2] ERIK EDSTRÖM,[1] OSCAR PERSSON,[1,2] AND ADRIAN ELMI-TERANDER[1,2,6]

[1]*Department of Neurosurgery, Karolinska University Hospital, 171 64 Stockholm, Sweden*
[2]*Department of Clinical Neuroscience, Karolinska Institutet, 171 77 Stockholm, Sweden*
[3]*Philips Research, 5656 AE, Eindhoven, The Netherlands*
[4]*Eindhoven University of Technology (TU/e), Eindhoven, The Netherlands*
[5]*Department of Biomechanical Engineering, Delft University of Technology, 2628 CD, Delft, The Netherlands*
[6]*Stockholm Spine Center, 194 45 Upplands-Väsby, Sweden*
[*]*simon.skyrman@regionstockholm.se*

Abstract: Glial tumors grow diffusely in the brain. Survival is correlated to the extent of tumor removal, but tumor borders are often invisible. Resection beyond the borders as defined by conventional methods may further improve prognosis. In this proof-of-concept study, we evaluate diffuse reflectance spectroscopy (DRS) for discrimination between glial tumors and normal brain ex vivo. DRS spectra and histology were acquired from 22 tumor samples and nine brain tissue samples retrieved from 30 patients. The content of biological chromophores and scattering features were estimated by fitting a model derived from diffusion theory to the DRS spectra. DRS parameters differed significantly between tumor and normal brain tissue. Classification using random forest yielded a sensitivity and specificity for the detection of low-grade gliomas of 82.0% and 82.7%, respectively, and the area under curve (AUC) was 0.91. Applied in a hand-held probe or biopsy needle, DRS has the potential to provide intra-operative tissue analysis.

1. Introduction

Gliomas are intra-axial brain tumors with a diffusely invasive growth pattern. They are classified based on their histological type, such astrocytoma, oligodendroglioma or mixed, and their malignancy grade according to the world health organization (WHO) classification. Tumors classified as WHO I-II are considered low-grade gliomas (LGG) and III-IV high-grade gliomas (HGG). The diffuse transition from tumor to normal parenchyma makes complete surgical removal very challenging and most tumor relapses occur in the direct vicinity of the resection cavity where the concentration of tumor cells is the highest. Complete or near complete gross total resection (GTR) is one of the main predictors of a prolonged overall survival for these patients [1–3]. A major advance in neurosurgical technique during the last decades has been the development of fluorescence guided resections, leading to significantly improved GTR rates and patient outcomes [4,5]. In LGG, however, the accumulation of fluorescent agents is poorer as the blood-brain barrier is intact, and LGGs are harder to differentiate from normal tissue under normal light microscopy [6–8]. It is possible that extended resections beyond the tumor border as defined either by MRI, ultrasound or fluorescence could further improve outcomes [9]. However, extended resections may compromise the surrounding brain tissue and cause neurological deficits. Accurate intraoperative sensing techniques that are able to reliably differentiate between tumor

#474344 https://doi.org/10.1364/BOE.474344
Journal © 2022 Received 29 Aug 2022; revised 3 Nov 2022; accepted 6 Nov 2022; published 15 Nov 2022

Biomedical Optics EXPRESS

and healthy tissue within the resection cavity may provide the surgeon with the information needed to safely achieve GTR. As of today, no such sensing technique is in clinical use.

Frame-based or frameless stereotactic biopsies are performed on brain tumor patients that for different reasons cannot undergo tumor resection surgery. Despite navigation and that tissue samples deemed to be relevant are obtained in 90-95% of the biopsies, the diagnostic accuracy is significantly lower at 57-73% [10]. One reason for this discrepancy is that biopsies may be performed in less representative parts of the tumor. Intraoperative MRI, ultrasound or fluorescent tumor agents can be used to verify that a biopsy contains tumor material. However, these methods are costly, time consuming or applicable only to certain pathologies and may still fail to ensure a truly representative biopsy. The best way to confirm the representativity of a biopsy is a rapid histopathological examination of frozen sections. However, the turn-around time of a frozen section analysis is substantial and entails prolonged procedure time. Technologies able to verify that a biopsy needle is correctly positioned in a representative part of the target, in real time and before tissue sampling, would improve the diagnostic accuracy and workflow of these procedures.

Various applications of biomedical optics [11], including Raman spectroscopy [12], laser Doppler flowmetry [13] and confocal microscopy [14], have been investigated for the purpose of intra-operative tissue diagnostics in neurosurgery. Optical methods have several advantages, as they may provide real-time objective data and are easily integrated in surgical instruments [13,15]. Also, by including wavelengths outside the visual spectra, differences between tumor and normal brain that is not visible to the human eye may be captured. This study focuses on the optical method diffuse reflectance spectroscopy (DRS), where light is emitted into tissues via an optic fiber, and the back-scattered light is collected and analyzed spectroscopically. Since a specific tissue type has a unique composition of chromophores, the collected spectra act as an "optical fingerprint" for that specific tissue. DRS has been used successfully for tissue identification in experimental spinal surgery [16], interventional stroke research [17,18] and in studies on cancer diagnostics [19,20]. A previous feasibility study in a porcine model showed that DRS in combination with an automated classification algorithm could differentiate between white and grey matter in the CNS [21]. Attempts to use the technique to differentiate between gliomas and normal brain parenchyma or between different brain tissue types have shown promise, but no application for clinical use has been developed [22–29,30]. In previous studies, DRS was combined with fluorescence or auto-fluorescence spectroscopy and evaluated for glioma discrimination in the wavelength range of 300-800 nm. It has however proven hard to use DRS alone for accurate discrimination of glioma tissue. [26–29]

In this *ex-vivo* proof-of-concept study, DRS is evaluated for the development of a clinical tool for brain tumor identification discriminating between LGG and HGG and healthy brain tissue respectively. By including a broader wavelength spectrum (450-1600 nm), discriminative features for glioma detection in the near infrared spectrum are examined. Measurements are performed on glial tumor samples and compared to normal brain tissue samples from epilepsy surgery or healthy peritumoral tissue. The DRS data is analyzed, and its discriminative features are studied by the application of a machine learning classification algorithm. The model is able to discriminate LGG and HGG respectively from normal white and gray matter, based on DRS as a single modality.

2. Material and methods

The study hospital is a publicly funded and owned tertiary care center serving a region of roughly 2.3 million inhabitants, and the only neurosurgical center in the region. All patients undergoing surgery for brain tumor or epilepsy at the study center were eligible for inclusion. Those operated when a DRS operator (Burström G., Skyrman S.) was available were included in the study. Tumor tissue was acquired from neurosurgical operations of patients with intracranial tumors and healthy brain samples were collected from patients undergoing epilepsy surgery or from

Biomedical Optics EXPRESS

normal peritumoral tissue in tumor patients. All surgeries were conducted according to the standard protocols of the department. Patients with suspected glial tumors were administered 5-ALA orally 1 h before surgery. Signed informed consent was obtained from all participants or their legal guardians. The study was approved by the National Ethical Review Authority (Dnr 2018/794-32, 2018/2670-31/1, and 2019-00100).

The general principles of DRS, instrumentation and calibration have been described previously [31]. In short, light from a tungsten halogen broadband light source (360 to 2500 nm) is coupled to an optical multimode fiber (200 micron core diameter) integrated in a handheld probe. The light exits the fiber at the tip of the probe and reflected light from the examined tissue is collected by another optical fiber (Fig. 1). The distance between the fibers at the probe tip is 0.45 mm. The collecting fiber is split by a Y-junction into two separate fibers that are coupled to two spectrometers, of which one resolves light in the visible and near-infrared wavelength range of 450 to 1100 nm (OceanOptics Maya 2000PRO, Ocean Insight, Orlando, FL, USA), while another covers the infrared wavelengths from 900 to 1600 nm(OceanOptics NIRQuest512, Ocean Insight, Orlando, FL, USA). The measurements were acquired simultaneously from the same position for the two spectrometers. For the overlapping wavelengths obtained from both spectrometers (900-1100 nm), a matching factor was calculated to create a continuous spectrum from 450 and 1600 nm. For data acquisition and controlling of the spectrometers, a custom software developed in-house was used (Labview).

Immediately after removal, tumor samples were rinsed using saline and DRS measurements were performed in a dark room with the samples positioned on a black sheet of paper. Before each measurement session, the system was calibrated on a white reference (Spectralon), as previously described [31]. To avoid potential influence from probe positioning, measurements were obtained with the probe both perpendicular and parallel to the underlying black surface. The number of measurement positions per sample was determined by tissue size, with a minimum distance of 2 mm between each measurement position. Ten measurements were acquired at each position, and the total acquisition time for each position was 4.5 seconds. Measurement positions were documented on photographs of the samples, and each position was annotated as tumor tissue, healthy white matter or healthy grey matter as defined by the operating neurosurgeon (Fig. 1). The data were averaged using the median of the 10 measurements from each measurement position. For the classification, each measurement position was treated as an independent data point, i.e. data was not averaged per sample or patient.

After DRS-measurements, the tumor samples were immediately placed in 10% formalin and transferred to the pathology department, where histopathological analyses were performed according to the standard routine at the department. Tumor histology was reported according to the WHO classification. WHO grade I and II were classified as LGG and WHO grade III and IV as HGG.

DRS data acquired from the *ex-vivo* measurements were analyzed in the wavelength range of 450 to 1600 nm with a custom software using MATLAB (MathWorks Inc., Natick, MA). The DRS spectra were fitted with a previously described model derived from diffusion theory [31]. The model estimates the tissues' scattering features and concentrations of tissue chromophores, i.e. tissue constituents with strong light absorbing properties such as hemoglobin, water or fat. This requires knowledge of the wavelength-dependent absorption coefficients of the chromophores of interest, and the fiber distance between the emitting and collecting fibers. Due to the small fiber separation of the probe used in this study, the mathematical assumptions behind diffusion theory are no longer valid. As a result, values of $> 100\%$ were achieved for some fitted parameters. However, since the measurements in the study are performed with the same probe and under the exact same conditions for both normal and tumor tissue samples, the model can be assumed to be valid for discrimination between the samples based on the estimated relative content of different chromophores and scattering properties. Chromophores included in the analysis were

Biomedical Optics EXPRESS

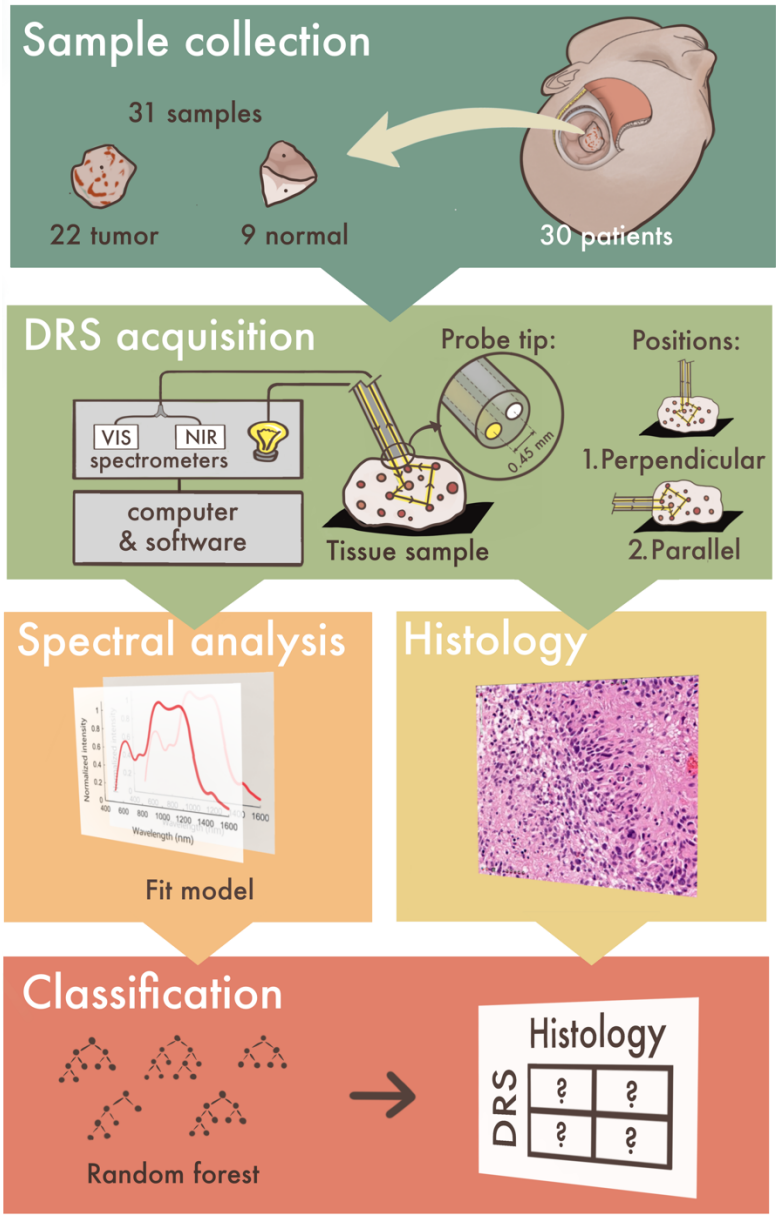

Fig. 1. Study design and the DRS system. Overview of the study design and DRS system. In short, 30 patients were included in the study, from which 31 tissue samples were acquired, 22 tumor and 9 normal brain samples. Samples were examined with DRS light from a tungsten halogen broadband light source (360 to 2500 nm) coupled to an optical multimode fiber (200 micron core diameter) integrated in a handheld probe. The light exits the fiber at the tip of the probe and reflected light from the examined tissue is collected by an identical optical fiber and lead to two spectrometers, one of which resolves light in the visible and near-infrared wavelength range of 450 to 1100 nm, and the other in the infrared wavelengths from 900 to 1600 nm. The distance between the fibers at the probe tip is 0.45 mm. A previously published optical model derived from diffusion theory was used for spectral analysis (fitting) of the DRS data. Finally, random forest classification based on the fitted DRS parameters was performed to examine the ability of DRS to predict the samples' histology.

Biomedical Optics EXPRESS

oxygenated hemoglobin (wavelength peak 450-600 nm), deoxygenated hemoglobin (450-600 and ≈760 nm), fat (930 and 1210 nm) and water (972, 1200 and 1400 nm) [32]. The hemoglobin oxygen saturation (StO2) was estimated. Since strong absorbers like hemoglobin tend to aggregate in distinct regions of biological tissue, a correction factor (Rves) corresponding to regional clustering of strong absorbers was analyzed, as previously described [33]. Estimates of the wavelength-dependent scattering contributions from Mie and Rayleigh scattering were calculated as described previously [31]. The reduced scattering coefficient (μ's(λ)) was estimated using an empirical model

$$\mu's(\lambda) = \mu's(\lambda 0)\left(Fmie\left(\frac{\lambda}{\lambda 0}\right)^{-b} + (1 - Fmie)\left(\frac{\lambda}{\lambda 0}\right)^{-4}\right).$$

A reference wavelength (λ0) of 800 nm was used, where the scaling factor μ's(λ0) corresponds to the reduced scattering amplitude at the specific wavelength, *Fmie* represents the Mie-to-Rayleigh fraction of scattering:, assuming that Mie and Rayleigh are the dominant forms of tissue scattering, and *b* corresponds to the Mie scattering slope.

After fitting of the spectra, the fitted data were tested for normality using Shapiro-Wilk test. Non-normal distributed data were log-transformed. The median of ten measurements at each measurement position was used for analysis. DRS data for the tissue were plotted in box plots and the independent t-test was used for calculation of statistically significant differences in mean values between the normal tissues and tumor types. Finally, a random forest classification model was applied for discrimination between the tissue types [34]. For training the random forest model, RStudio (RStudio Team. RStudio: Integrated Development for R. RStudio, Inc., Boston, USA) and the randomForest package was used [35]. A leave-one-out cross-validation method for training and testing the classification models was employed to avoid overfitting. In each round of training, an individual patient was chosen as the validation set, and the rest of the patient data was used for training by generating 500 decision trees. This was repeated until all patients' data had acted as a validation set. All classification models were trained using the same input parameters (500 decision trees, 2 variables randomly sampled at each split, tree grown until terminal node size of 1) and the same fit parameters (all nine parameters from the fit model described above). No hyperparameter tuning was performed. Receiver operating characteristic (ROC)-curves were generated using an approximation suitable for random forest data using the pROC package [36]. Since the implementation of random forests does not provide a true probability output, sample tree classification votes were used as an approximation of a probability value to generate ROC-curves. The ROC-curves presented are the combined curves for prediction of LGG and HGG tumors, respectively, and contain all true values from the random forest models. For each classifier an averaged ROC-curve was generated, based on 30 approximated ROC-curves from the leave-one-out-analyses.

All results are presented as median (absolute range).

3. Results

3.1. Patient data

A total of 30 patients were included. Glial tumor samples were retrieved from 22, of which 6 from LGG and 16 from HGG, and normal tissue from 9 patients. The normal tissue was acquired from epilepsy surgery in 6 cases, and from normal peritumoral brain tissue in patients operated for brain tumor in 3 cases (Table 1). Median sample length and width were 10 (3-22) and 6 (3-13) mm respectively. Sample thickness was > 3 mm for all samples.

Biomedical Optics EXPRESS

Table 1. Patient and sample data. Demographic patient data and summary of tissue samples. Notably, patients in the normal tissue group were significantly younger than patients in the tumor group (median age 22 vs 48), reflecting the different age distributions of tumor and epilepsy diagnoses in the population. A total of 30 patients were included. From three patients, one with a well demarcated glioblastoma and two with metastases, both tumor and normal tissue were resected.

	Glial tumor	Normal tissue	Significance
Samples (n)	**22**	**9**	**-**
Patient age (median, range)	**48 (17-75)**	**22 (2-67)**	**p = 0.02**
Patient sex (% female)	**57.1**	**53.3**	**p = 0.8**
Diagnosis (n)			**-**
Glial tumor	**22**		
Epilepsy		**6**	
Peritumoral tissue		**3**	
Number of samples per tissue diagnosis (n)			**-**
LGG			
Diffuse glioma (WHO II)	**6**		
HGG			
Anaplastic glioma (WHO III)	**3**		
Glioblastoma (WHO IV)	**13**		
Normal tissue			
White		**6**	
Grey		**9**	
Number of measurement positions per tissue diagnosis (n)			**-**
LGG			
Diffuse glioma (WHO II)	**61**		
HGG			
Anaplastic glioma (WHO III)	**48**		
Glioblastoma (WHO IV)	**163**		
Normal tissue			
White		**36**	
Grey		**61**	

3.2. DRS measurements and fitting results

Ten consecutive DRS measurements were acquired at each of a total of 369 measurement positions. Among these, 61 were in grey matter, 36 in white matter and 272 in solid glial tumor tissue, of which 61 in LGG and 211 in HGG. Median measurement positions per tissue sample was 11 (4-26). Averaged spectra for white matter, grey matter and glial tumors are shown in Fig. 2. Spectra form all tissues had notable valleys at 450-600 nm, representing blood content and/or microscopic blood contamination of the tissues. As expected, white matter spectra were influenced by high fat content, with valleys at approximately 930 and 1210 nm. White matter also had the highest scattering coefficient, corresponding to the highly reflective properties of white matter tracts. For the other tissues, the scattering and mean intensity increased with the cellularity of the examined tissues, with grey matter and LGG tumor showing lower scattering coefficients than the cell-rich tumors of higher grades.

Biomedical Optics EXPRESS

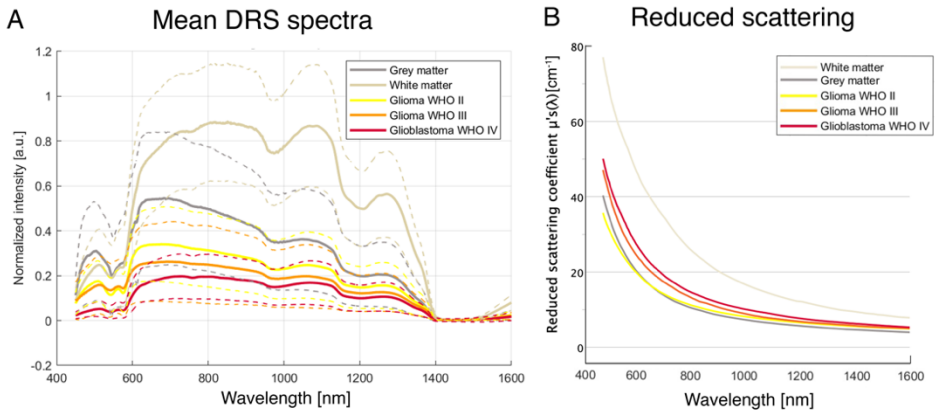

Fig. 2. 2a Averaged DRS spectra with the standard deviation presented as dotted lines. 2b Averaged reduced scattering coefficient.

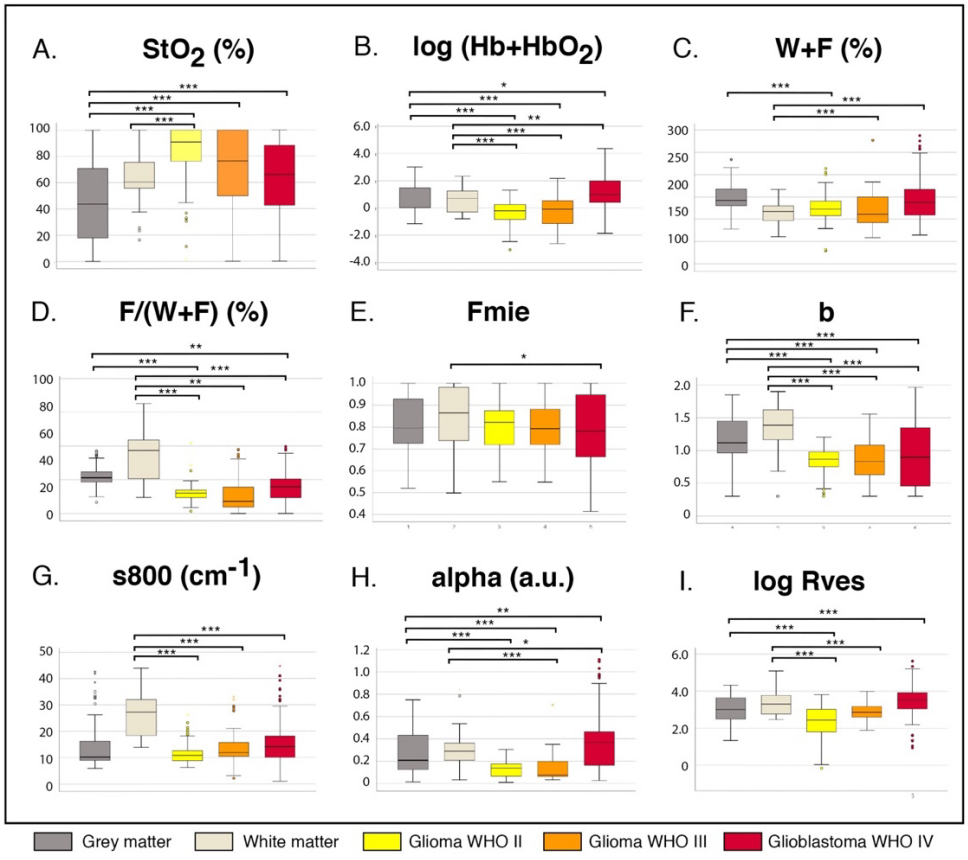

Fig. 3. Boxplots of the DRS parameters derived from the fit model. Significantly differences in mean values are indicated with brackets where * p ≤0,05, ** p ≤0,01 and *** p ≤ 0,001.

The physiological differences between the tissues as estimated by fitted DRS parameters are presented as boxplots in Fig. 3. Most of the parameters showed statistically significant differences between glial tumor tissue and white and grey matter. Estimated tissue oxygenation

Biomedical Optics EXPRESS

(StO_2) was higher in tumor tissues of all grades than in grey matter, and higher in WHO II gliomas compared to white matter (Fig. 3(a)). Estimated content of blood ($Hb + HbO_2$) showed significant differences between tumors of all grades and both white and grey matter (Fig. 3(b)). Fat (F) and water (W) content as estimated by DRS are presented in Fig. 3(c) and 3d. The F/(F + W)-ratio differed significantly between tumor and white and grey matter except for grey matter and WHO III gliomas. Regarding scattering, the contribution of Mie scattering (Fmie, Fig. 3(e)) only showed a significant difference between white matter and glioblastoma, whereas the Mie slope parameter b (Fig. 3(f)) displayed larger differences between all tumor types vs grey and white matter respectively. Alpha, S800 and the clustering correction factor Rves also displayed potentially discriminative features between tumor and normal brain tissue, as presented in Fig. 3(g)-(i).

3.3. Random forest classification

A random forest classification based on all nine above-presented DRS fit parameters. A sensitivity of 82.0% and specificity of 82.7% was achieved for detection of LGG vs normal brain tissue. The result of the classification is presented as a confusion matrix in Table 2 and as an approximated ROC curve in Fig. 4(a), where the area under curve (AUC) was 0.91. Classification of HGG tumor vs normal brain tissue reached a high sensitivity (93.3%) but a low specificity (43.2%), as shown in the confusion matrix (Table 3) and approximated ROC curve (Fig. 4(b)).

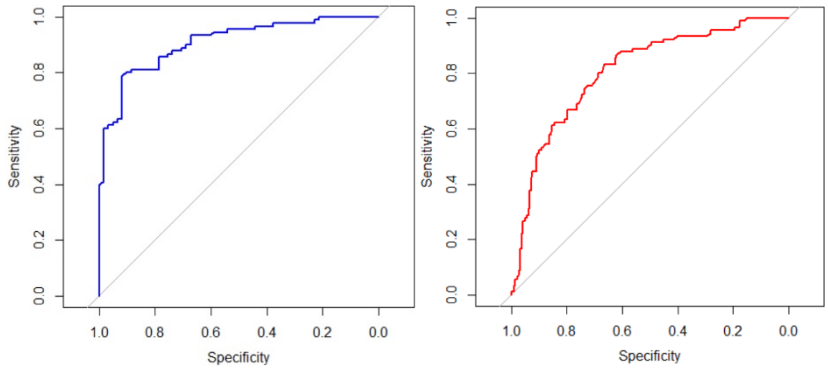

Fig. 4. Result of random forest classification presented as ROC curves. Approximated receiver operating characteristic (ROC) curves for prediction of a) LGG and b) HGG based on the nine DRS fit parameters. The curves illustrate the trade-off between sensitivity (y-axis) and specificity, (x-axis), for every possible cut-off value. AUC was 0.91 and 0.81 respectively.

Table 2. Classification of low-grade glioma vs normal grey and white matter. Confusion matrices of the results of the random forest classification for LGG vs normal grey and white matter. The result of the histological examination is presented in the columns, and the tissue type prediction by the random forest model is presented in the rows. Correct predictions are highlighted in white.

		Histological tissue diagnosis		
		LGG	Grey matter	White matter
DRS classification diagnosis	**LGG**	50	7	4
	Grey matter	8	22	5
	White matter	3	6	30

Biomedical Optics EXPRESS

Table 3. Classification of high-grade glioma vs normal grey and white matter. Confusion matrices of the results of the random forest classification for HGG vs normal grey and white matter. The result of the histological examination is presented in the columns, and the tissue type prediction by the random forest model is presented in the rows. Correct predictions are highlighted in white.

		Histological tissue diagnosis		
		HGG	Grey matter	White matter
DRS classification diagnosis	**HGG**	197	26	16
	Grey matter	2	9	0
	White matter	12	0	23

4. Discussion

We hypothesized that DRS can be used as an intraoperative sensor for glial tumors. In this proof-of-concept study the ability of DRS to discriminate between glial tumor tissue of different grades and normal brain tissue was investigated *ex-vivo*. Evident differences between the mean spectra of the different tissue types were seen. These differences may be attributed to structural changes both at a subcellular level, such as changes of cell membranes and mitochondrial features, or at tissue level, like neovascularization or the general level of cellularity of the tissue, where the latter is expected to be the lowest in white matter and the highest in glioblastoma (Fig. 2(a)). The reduced scattering coefficient ($\mu's$) (Fig. 2(b)) demonstrated decreasing values with increasing wavelengths, which has been described as a typical feature in previously published results in human [23,37] and rat brain [38]. Previous results of $\mu's$ in relation to glioma tumor grade have been conflicting, where both reports of higher values for higher grade tumors than lower grade tumors [23] (like the results of this current study) and the opposite [37] have been reported. Furthermore, significant differences between normal brain and tumor tissue were seen in most of the fitted DRS parameters (Fig. 3), indicating that the concentration of major tissue constituents and scattering properties can be estimated by DRS measurements. The results of the fit model are in line with previous descriptions of chromophore content and optical properties of brain and glioma tissue. A clear pattern of decreased tissue oxygenation as estimated by DRS with increasing tumor grade was seen (3a), in line with studies on glioma and hypoxia [39]. DRS derived estimates of oxygenized and deoxygenized hemoglobin, reflecting the tissue blood content, were lower in grade II glioma than normal tissue, and clearly higher in grade IV gliomas than in normal tissue (Fig. 3(b)), as previously reported [40]. This result also corresponds to radiological measurements of blood flow in glioma tissue. [41]. In accordance with previous studies, the DRS fat parameter was reduced in gliomas, while DRS estimates of water content were higher in gliomas than normal tissue (Fig. 3(c) and 3(d)). [42]. Since fat and water have strong absorption bands in the near infra-red spectrum, the inclusion of wavelengths up to 1600 nm in the current study may better take advantage of this glioma feature than previous studies where only wavelengths below 800 nm were included. The high refractive index of white matter, caused by the multi layered lipid membranes of myelinated nerves, was evident in the DRS scattering parameters (Fig. 3(e)-(h)), and was decreased in glioma tissue, likely due to invasion of tumor cells into the white matter tracts.

Based on the fitted parameters, a random forest classification model was trained to discriminate healthy brain tissue from LGG with a sensitivity and specificity of 82.0% and 82.7% respectively and an AUC of 0.91, despite the limited clinical material. The model did not perform as well for classification of HGG vs healthy brain tissue (sensitivity 93.3%, specificity of 43.2%, AUC 0.81). The skewness of the results may partly be attributed to the uneven number of measurements of normal tissue (97) vs HGG (211), but could also possibly reflect a higher degree of histological

Biomedical Optics EXPRESS

heterogenicity; HGG has both highly proliferative cell dense areas and, in the case of glioblastoma, regions with necrosis.

The results of this study are in line with previous publications and further support the potential use of DRS for glial tumor detection [23,25–29]. An overview of previously published data on DRS for brain tumor discrimination is presented in Table 4. The reported sensitivity and specificity for discrimination of gliomas from normal human brain have varied between 80-100% and 89-96% respectively [23,25–29,30]. However, these results are not directly comparable to the current study for several reasons. In all previous studies, DRS was used in combination with a second modality, either spectroscopic measurements of auto-fluorescence [23,25–28,30] or 5ALA-fluorescence [29]. DRS used alone has in fact not previously been demonstrated to be able to discriminate between gliomas and healthy brain, possibly due to difficulties in differentiating tumor from grey matter [25,30]. In the current study, classification based on DRS reached an accuracy comparable to previous dual modality studies. It is likely that an even higher accuracy could be reached by adding a second modality to the DRS method described in this study. Several optical techniques show promising results and could be used for this purpose, including the above mentioned auto-fluorescence spectroscopy [23,25–28,30] and 5ALA-fluorescence spectroscopy [29], as well as Raman spectroscopy [43,44] and laser Doppler flowmetry [13].

Table 4. Publications on DRS for glioma detection. Overview of previous publications of DRS for glioma detection.

Publication	In/ex vivo	Tissue types	DRS range (nm)	Sample size (patients/ positions)	Modality	Analysis	Sensitivity /specificity normal brain vs solid glioma (%)
Lin et al 2000 [25]	ex	Normal Glioma Metastasis	400-800	20/120	DRS + autofluorescence	Empirical discrimination algorithm	97/96
Lin et al 2001 [26]	in	Normal Glioma Metastasis	400-800	26/120	DRS + autofluorescence	Empirical discrimination algorithm	84/NR
Toms et al 2005 [28]	in	Normal Glioma	400-800	35/230	DRS + autofluorescence	Empirical discrimination algorithm	80/89
Valdés et al 2011 [29]	in	Normal Glioma	450-720	10/264	DRS + 5ALA-fluorescence	Model derived fit parameters + SVM[a]	94/94
Majumder et al 2007 [27]	in	Normal Glioma	400-800	24/184	DRS + autofluorescence	MRDF + SMLR[b]	NR
Du Le et al 2017 [23]	ex	Glioma	430-700	7/22	DRS + autofluorescence	Empirical discrimination algorithm	NR
Lu et al 2021 [30]	ex	Normal Glioma	300-700	5/180	DRS + autofluorescence	PLS-LDA + LOOCV[c]	89.3/92.5
Skyrman et al 2022 (Current study)	**ex**	**Normal Glioma**	**450-1600**	**30/369**	**DRS only**	**Model derived fit parameters + RF[d]**	**82.0/82.7**

[a]Support vector machine,
[b]Maximum representation and discrimination feature + sparse multinomial logistic regression,
[c]Partial least square-linear discriminant analysis + leave-one-out cross validation
[d]Random forest classification. NR = not reported.

Biomedical Optics EXPRESS

Moreover, most of the previous studies employed empirical classifications models, where cutoff values at a single or a few selected wavelengths were chosen to maximize discrimination in the specifically studied data set [24–26,28,30]. Such classification models have several drawbacks including creating a bias towards the specific study population, as well as excluding possibly important information from other parts of the spectra than the specific wavelengths chosen. Two previous studies have applied more advanced algorithms based on Bayesian probability algorithms [27] or machine learning [29] with promising results. In the current study, a previously validated model based on diffusion theory was fitted to the spectra to derive estimates of tissue constituents, and a standard machine-learning method (random forest) was used for classification. Thus, there were no specific adaptions of the method to the specific data set, and thereby less risk of bias.

While previous studies have examined the visible spectrum and the lower end of the near infrared spectrum, wavelengths above 850 nm were not included. To the best of our knowledge, the current study is the first where a larger spectral range of 450–1600 nm has been used for human glial tumor detection. Including a larger portion of the near infrared spectrum may have several benefits. Firstly, it may detect differences between tumor and normal brain that is not visible to the human eye in an operating microscope. This is supported by the results in the current study, where several features that contributed to the discrimination between tissue types were seen in the spectrum above 1000 nm, including water and fat content. Secondly, tissue penetration depth in the near infrared spectrum is higher than in the visible range [45]. Based on the optic properties of normal brain and glioma tissue, probe design and the investigated wavelength spectrum, the measurement depth/probing volume for this DRS application is estimated to be approximately half of the fiber distance of 0.45 mm. This relatively short source to detector distance limits the measurement depth when measuring on the surface, however it allows for miniaturization and fitting of the application into a handheld probe that can be inserted into the tissue for measurements at different depths of the surgical field. This possibility enables acquisition of sub surface measurements, going beyond what can be achieved with an ordinary surgical microscope. Combined with image guided surgery systems or intraoperative ultrasound, these DRS measurements could provide a clinically valuable tool for the surgeon to optimize tumor resection, especially in the clinically challenging task of discriminating non-fluorescent LGGs from normal brain tissue. The minimally detectable tumor volume needed to yield a positive signal requires further investigation. This must be fine-tuned with cut-off values for the DRS signal, a topic outside the scope of this proof-of-concept study.

In summary, we have demonstrated that a standalone DRS probe using a spectral range of 450–1600 nm, shows promising results for discrimination between low- and high-grade glioma and healthy brain tissue in an ex vivo set-up.

5. Limitations

This study was performed on *ex-vivo* samples from a limited number of patients treated according to the normal clinical routine of a neurosurgical department. In order not to interfere with the department's tissue handling and diagnostic routine, no detailed correlation of the exact DRS measurement position with histology at the exact same position were made. Instead, samples were treated as larger volumes of homogenous tumor or normal tissue and labeled as such. Since glioma tissue is heterogenous in nature, this method does not likely reflect the maximal potential accuracy of DRS for tumor detection. On the other hand, it represents well the conditions met in a real-life scenario during tumor surgery, where larger volumes of tissue need to be examined and resected.

For the classification model, measurements at different positions of the same samples were treated as independent data points, i.e. data was not averaged per sample or patient. This was considered justified since a leave-one-out methodology was used in the random forest

Biomedical Optics EXPRESS

classification, where data from patients in the validation set was excluded from the training set. Also, a high intra-individual variation was noted for each sample, while samples of the same tissue type (diagnosis) but from different patients exposed extensive overlaps of the DRS parameter values.

The fit model did not include the exogenic fluorescent agent and 5-ALA precursor PPIX, which was administered to patients with gliomas pre-operatively. Even though the main absorption band for PPIX (around 410 nm) is below the spectrum analyzed in this manuscript, absorption overlap that of hemoglobin and its derivates to some extent, and emission peaks from PPIX at approximately 630 nm and 700 nm respectively might have affected the spectra acquired from HGG in particular. In a future application, adding PPIX as a DRS fit parameter may further sharpen the analysis.

Except for one patient from which both tumor and normal tissue were extracted, in this study normal brain and tumor samples were retrieved from different individuals. Hence, variations of tissue composition between individual patients may have affected the results. To eliminate inter-individual variation and increase discrimination power in a future clinical application, the surgeon may first make a reference measurement on the patient's normal brain tissue for probe calibration, after which deviation from this normal measurement can be used for tumor identification in the same patient.

In this *ex-vivo* study, blood content may not represent the true conditions in vivo, and tissue oxygen saturation may have been affected by the period of air exposure between removal and DRS acquisition. Also, the sample size of especially normal brain tissue was limited, which reduces the generalizability of the results. The skewness of the data may to some extent have affected the classification. Adding a weight factor, or sub-sampling, could possibly have improved the results further.

6. Future development

This proof-of-concept study support the use of DRS for glial tumor detection. To translate the results into a clinically useful tool, further investigations are needed. In-vivo animal studies are planned for precise correlation of DRS measurements and histology in blood perfused tissue. An investigational device for use in clinical studies with larger sample sizes will be developed, possibly with integration of a second modality as discussed above. The goal will be to create a tissue bank with correlating DRS measurements. Based on data from a large sample size, more robust tissue classification algorithms could be developed. Finally, automated diagnostic evaluation and an interface for real-time feedback to the operating neurosurgeon must be developed.

7. Conclusion

In this proof-of-concept study the ability of DRS to discriminate between glial tumor tissue of different grades and normal brain tissue was investigated *ex-vivo*. Significant differences in the recorded DRS parameters were seen between normal brain and tumor tissue. Despite the limited sample size, a classification model based on DRS parameters could discriminate between low grade glioma and normal brain tissue. Further studies are warranted to evaluate the potential role of the technique as an intra-operative tissue sensing tool for tumor recognition in glioma surgery.

Funding. Stockholms Läns Landsting (FoUI-952709, FoUI-953669).

Acknowledgements. There are no acknowledgements.

Disclosures. None of the authors who are affiliated with clinical institutions or universities (S.S., G.B., F.M., A.F., E.E., O.P., A.E.-T) have financial interests in the subject matter, materials, or equipment or with any competing materials and did not receive any payments from Philips. Karolinska University hospital and Philips have a major collaboration agreement. The authors affiliated with Philips Research (M.L., B.H.) have financial interests in the subject matter, materials, and equipment, in the sense that they are employees of Philips. Philips provided support in the form of salaries

Biomedical Optics EXPRESS

but did not have any additional role in the study design, data collection and analysis, decision to publish, or preparation of the manuscript. Authors without conflicts of interest had full control of all data labelling, data analysis and information submitted for publication and over all conclusions drawn in the manuscript.

Data availability. Data underlying the results presented in this paper are not publicly available at this time but may be obtained from the authors upon reasonable request.

References

1. R. S. D'Amico, Z. K. Englander, P. Canoll, and J. N. Bruce, "Extent of resection in glioma-a review of the cutting edge," World Neurosurg. **103**, 538–549 (2017).
2. Q. Han, H. Liang, P. Cheng, H. Yang, and P. Zhao, "Gross total vs. subtotal resection on survival outcomes in elderly patients with high-grade glioma: a systematic review and meta-analysis," Front Oncol. **10**, 151 (2020).
3. S. L. Hervey-Jumper and M. S. Berger, "Maximizing safe resection of low- and high-grade glioma," J. Neurooncol. **130**(2), 269–282 (2016).
4. C. Orillac, W. Stummer, and D. A. Orringer, "Fluorescence guidance and intraoperative adjuvants to maximize extent of resection," Neurosurg. **89**(5), 727–736 (2021).
5. L. M. Wang, M. A. Banu, P. Canoll, and J. N. Bruce, "Rationale and clinical implications of fluorescein-guided supramarginal resection in newly diagnosed high-grade glioma," Front Oncol. **11**, 666734 (2021).
6. B. K. Hendricks, N. Sanai, and W. Stummer, "Fluorescence-guided surgery with aminolevulinic acid for low-grade gliomas," J. Neuro-Oncol. **141**(1), 13–18 (2019).
7. M. Jaber, C. Ewelt, J. Wölfer, B. Brokinkel, C. Thomas, M. Hasselblatt, O. Grauer, and W. Stummer, "Is visible aminolevulinic acid-induced fluorescence an independent biomarker for prognosis in histologically confirmed (World Health Organization 2016) low-grade gliomas?" Neurosurg. **84**(6), 1214–1224 (2019).
8. G. Widhalm, J. Olson, J. Weller, J. Bravo, S. J. Han, J. Phillips, S. L. Hervey-Jumper, S. M. Chang, D. W. Roberts, and M. S. Berger, "The value of visible 5-ALA fluorescence and quantitative protoporphyrin IX analysis for improved surgery of suspected low-grade gliomas," J. Neurosurg. **133**(1), 79–88 (2020).
9. H. Duffau, "Long-term outcomes after supratotal resection of diffuse low-grade gliomas: a consecutive series with 11-year follow-up," Acta Neurochir. **158**(1), 51–58 (2016).
10. S. Khatab, W. Spliet, and P. A. Woerdeman, "Frameless image-guided stereotactic brain biopsies: emphasis on diagnostic yield," Acta Neurochir. **156**(8), 1441–1450 (2014).
11. P. A. Valdés, D. W. Roberts, F.-K. Lu, and A. Golby, "Optical technologies for intraoperative neurosurgical guidance," Neurosurg. focus **40**(3), E8 (2016).
12. M. Jermyn, K. Mok, J. Mercier, J. Desroches, J. Pichette, K. Saint-Arnaud, L. Bernstein, M.-C. Guiot, K. Petrecca, and F. Leblond, "Intraoperative brain cancer detection with Raman spectroscopy in humans," Sci. Transl. Med. **7**(274), 274ra219 (2015).
13. N. Haj-Hosseini, J. C. O. Richter, P. Milos, M. Hallbeck, and K. Wårdell, "5-ALA fluorescence and laser Doppler flowmetry for guidance in a stereotactic brain tumor biopsy," Biomed. Opt. Express **9**(5), 2284–2296 (2018).
14. E. Belykh, C. Cavallo, S. Gandhi, X. Zhao, D. Veljanoski, N. Martirosyan, V. Byvaltsev, J. Eschbacher, M. Preul, and P. Nakaji, "Utilization of intraoperative confocal laser endomicroscopy in brain tumor surgery," J. Neurosurg. Sci. **62**(6), 704–717 (2018).
15. G. Burström, A. Swamy, J. W. Spliethoff, C. Reich, D. Babic, B. H. Hendriks, H. Skulason, O. Persson, A. E. Terander, and E. Edström, "Diffuse reflectance spectroscopy accurately identifies the pre-cortical zone to avoid impending pedicle screw breach in spinal fixation surgery," Biomed. Opt. Express **10**(11), 5905–5920 (2019).
16. A. Swamy, J. W. Spliethoff, G. Burström, D. Babic, C. Reich, J. Groen, E. Edström, A. Elmi-Terander, J. M. Racadio, and J. Dankelman, "Diffuse reflectance spectroscopy for breach detection during pedicle screw placement: a first in vivo investigation in a porcine model," BioMed. Eng. OnLine **19**(1), 47 (2020).
17. S. Skyrman, G. Burström, O. Aspegren, D. Babic, G. Lucassen, E. Edström, F. Arnberg, M. Ohlsson, M. Mueller, and A. Elmi-Terander, "Clot composition characterization using diffuse reflectance spectroscopy in acute ischemic stroke," Biomed. Opt. Express **13**(6), 3311–3323 (2022).
18. S. Skyrman, G. Burström, O. Aspegren, G. Lucassen, A. Elmi-Terander, E. Edström, F. Arnberg, M. Ohlsson, M. Mueller, and T. Andersson, "Identifying clot composition using intravascular diffuse reflectance spectroscopy in a porcine model of endovascular thrombectomy," J. NeuroIntervent. Surg. **14**(3), 304–309 (2022).
19. N. M. Štorkánová, S. Maryam, M. Amissah, H. Lu, N. Lynch, S. Killeen, M. O'Riordain, and S. Andersson-Engels, "Evaluation of wavelength ranges and tissue depth probed by diffuse reflectance spectroscopy for colorectal cancer detection," Sci. Rep. **11**(1), 1–17 (2021).
20. L. L. de Boer, T. M. Bydlon, F. Van Duijnhoven, M.-J. T. Vranken Peeters, C. E. Loo, G. A. Winter-Warnars, J. Sanders, H. J. Sterenborg, B. H. Hendriks, and T. J. Ruers, "Towards the use of diffuse reflectance spectroscopy for real-time in vivo detection of breast cancer during surgery," J. Transl. Med. **16**(1), 367 (2018).
21. M. Lai, S. Skyrman, C. Shan, E. Paulussen, F. Manni, A. Swamy, D. Babic, E. Edstrom, O. Persson, and G. Burstrom, "Automated classification of brain tissue: comparison between hyperspectral imaging and diffuse reflectance spectroscopy," Proc. SPIE **11315**, 113151X (2020).
22. J. Antonsson, O. Eriksson, P. Blomstedt, A. T. Bergenheim, M. I. Hariz, J. Richter, P. Zsigmond, and K. Wårdell, "Diffuse reflectance spectroscopy measurements for tissue-type discrimination during deep brain stimulation," J. Neural Eng. **5**(2), 185–190 (2008).

Biomedical Optics EXPRESS

23. V. N. Du Le, J. Provias, N. Murty, M. S. Patterson, Z. Nie, J. E. Hayward, T. J. Farrell, W. McMillan, W. Zhang, and Q. Fang, "Dual-modality optical biopsy of glioblastomas multiforme with diffuse reflectance and fluorescence: ex vivo retrieval of optical properties," J. Biomed. Opt. **22**(2), 027002 (2017).
24. W.-C. Lin, D. I. Sandberg, S. Bhatia, M. D. Johnson, S. Oh, and J. Ragheb, "Diffuse reflectance spectroscopy for in vivo pediatric brain tumor detection," J. Biomed. Opt. **15**(6), 061709 (2010).
25. W.-C. Lin, S. A. Toms, M. Motamedi, E. D. Jansen, and A. Mahadevan-Jansen, "Brain tumor demarcation using optical spectroscopy: an in vitro study," J. Biomed. Opt. **5**(2), 214–220 (2000).
26. W. C. Lin, S. A. Toms, M. Johnson, E. D. Jansen, and A. Mahadevan-Jansen, "In vivo brain tumor demarcation using optical spectroscopy," Photochem. Photobiol. **73**(4), 396–402 (2001).
27. S. K. Majumder, S. Gebhart, M. D. Johnson, R. Thompson, W.-C. Lin, and A. Mahadevan-Jansen, "A probability-based spectroscopic diagnostic algorithm for simultaneous discrimination of brain tumor and tumor margins from normal brain tissue," Appl. Spectrosc. **61**(5), 548–557 (2007).
28. S. A. Toms, W. C. Lin, R. J. Weil, M. D. Johnson, E. D. Jansen, and A. Mahadevan-Jansen, "Intraoperative optical spectroscopy identifies infiltrating glioma margins with high sensitivity," Neurosurgery **57**(2), 382–394 (2005).
29. P. A. Valdés, F. Leblond, K. D. Paulsen, A. Kim, B. C. Wilson, O. M. Conde, B. T. Harris, and D. W. Roberts, "Combined fluorescence and reflectance spectroscopy for in vivo quantification of cancer biomarkers in low-and high-grade glioma surgery," J. Biomed. Opt. **16**(11), 116007 (2011).
30. H. Lu, K. Grygoryev, N. Bermingham, M. Jansen, M. O'Sullivan, G. Nunan, K. Buckley, K. Manley, R. Burke, and S. Andersson-Engels, "Combined autofluorescence and diffuse reflectance for brain tumour surgical guidance: initial ex vivo study results," Biomed. Opt. Express **12**(4), 2432–2446 (2021).
31. R. Nachabé, B. H. Hendriks, G. W. Lucassen, M. van der Voort, D. J. Evers, E. J. Rutgers, M.-J. V. Peeters, J. A. Van der Hage, H. S. Oldenburg, and T. J. Ruers, "Diagnosis of breast cancer using diffuse optical spectroscopy from 500 to 1600 nm: comparison of classification methods," J. Biomed. Opt. **16**(8), 087010 (2011).
32. T. M. Bydlon, R. Nachabé, N. Ramanujam, H. J. Sterenborg, and B. H. Hendriks, "Chromophore based analyses of steady-state diffuse reflectance spectroscopy: current status and perspectives for clinical adoption," J. Biophotonics **8**(1-2), 9–24 (2015).
33. N. Rajaram, A. Gopal, X. Zhang, and J. W. Tunnell, "Experimental validation of the effects of microvasculature pigment packaging on in vivo diffuse reflectance spectroscopy," Lasers Surg. Med. **42**(7), 680–688 (2010).
34. Y. Qi, "Random Forest for Bioinformatics," in *Ensemble Machine Learning: Methods and Applications*, C. Zhang and Y. Ma, eds. (Springer, US, 2012), pp. 307–323.
35. A. Liaw and M. Wiener, "Classification and regression by randomForest," R news **2**, 18–22 (2002).
36. X. Robin, N. Turck, A. Hainard, N. Tiberti, F. Lisacek, J.-C. Sanchez, and M. Müller, "pROC: an open-source package for R and S + to analyze and compare ROC curves," BMC Bioinformatics **12**(1), 77 (2011).
37. J. Shapey, Y. Xie, E. Nabavi, M. Ebner, S. R. Saeed, N. Kitchen, N. Dorward, J. Grieve, A. W. McEvoy, and A. Miserocchi, "Optical properties of human brain and tumour tissue: An ex vivo study spanning the visible range to beyond the second near-infrared window," J. Biophotonics **15**(4), e202100072 (2022).
38. E. A. Genina, A. N. Bashkatov, D. K. Tuchina, P. A. Dyachenko, N. Navolokin, A. Shirokov, A. Khorovodov, A. Terskov, M. Klimova, and A. Mamedova, "Optical properties of brain tissues at the different stages of glioma development in rats: pilot study," Biomed. Opt. Express **10**(10), 5182–5197 (2019).
39. S. M. Evans, K. D. Judy, I. Dunphy, W. T. Jenkins, W.-T. Hwang, P. T. Nelson, R. A. Lustig, K. Jenkins, D. P. Magarelli, S. M. Hahn, R. A. Collins, M. S. Grady, and C. J. Koch, "Hypoxia Is important in the biology and aggression of human glial brain tumors," Clin. Cancer Res. **10**(24), 8177–8184 (2004).
40. T. A. Savelieva, I. D. Romanishkin, Y. S. Maklygina, P. V. Grachev, N. A. Kalyagina, A. V. Borodkin, A. V. Orlov, B. A. Tsarukaev, A. A. Aristov, A. V. Kosyrkova, S. A. Goryajnov, S. V. Shugaj, L. V. Shishkina, A. A. Potapov, and V. B. Loschenov, "Optical biopsy: fundamentals and applications in neurosurgery," J. Phys.: Conf. Ser. **2058**(1), 012024 (2021).
41. L. Guida, V. Stumpo, J. Bellomo, C. H. B. van Niftrik, M. Sebök, M. Berhouma, A. Bink, M. Weller, Z. Kulcsar, L. Regli, and J. Fierstra, "Hemodynamic imaging in cerebral diffuse glioma–part a: concept, differential diagnosis and tumor grading," Cancers **14**(6), 1432 (2022).
42. M. Köhler, S. Machill, R. Salzer, and C. Krafft, "Characterization of lipid extracts from brain tissue and tumors using Raman spectroscopy and mass spectrometry," Anal. Bioanal. Chem. **393**(5), 1513–1520 (2009).
43. J. Desroches, M. Jermyn, K. Mok, C. Lemieux-Leduc, J. Mercier, K. St-Arnaud, K. Urmey, M.-C. Guiot, E. Marple, and K. Petrecca, "Characterization of a Raman spectroscopy probe system for intraoperative brain tissue classification," Biomed. Opt. Express **6**(7), 2380–2397 (2015).
44. J. Wahl, E. Klint, M. Hallbeck, J. Hillman, K. Wårdell, and K. Ramser, "Raman spectroscopic analysis of fresh tissue samples from brain tumors," in *European Conferences on Biomedical Optics 2021 (ECBO)* (Optica Publishing Group, Munich, 2021), p. EM1A.1.
45. A. Yaroslavsky, P. Schulze, I. Yaroslavsky, R. Schober, F. Ulrich, and H. Schwarzmaier, "Optical properties of selected native and coagulated human brain tissues in vitro in the visible and near infrared spectral range," Phys. Med. Biol. **47**(12), 3052059 (2002).